VORTEX-INDUCED VIBRATIONS BY AXIAL FLOW IN A BUNDLE OF CYLINDERS

Jeroen De Ridder *
Joris Degroote
Jan Vierendeels
UGent
Department of Flow, Heat and Combustion Mechanics
Sint-Pietersnieuwstraat 41
9000 Gent, Belgium
E-mail: {j.deridder,joris.degroote,
jan.vierendeels}@ugent.be

Katrien Van Tichelen

SCK-CEN
Boeretang 200
2400 Mol, Belgium
E-mail: kvtichel@sckcen.be

ABSTRACT

This contribution investigates the occurrence of vortex streets caused by axial flow in bundles of cylinders and the vibrations they trigger using numerical simulations. The vortex streets originate from the difference in axial flow speed in the gap between cylinders and the subchannel center. The dependence of this flow instability on typical parameters such as mean convection velocity and pitch-over-diameter ratio will be investigated. In a following part, two way coupled fluid-structure interaction simulations will be used to predict the vibration of flexible cylinders mounted in these channels. These simulations show that cylinders at the border of the bundle experience stronger oscillations. The influence of stiffness on vibrational amplitude is also tested in a parameter sweep.

NOMENCLATURE

D Diameter of the cylinder
D_H Hydaulic diameter
E Young's modulus
f Frequency
F Force
G Gap between cylinder and hex can
I Second area moment
L Length
M Mass
P Pitch - distance between center of two neighboring cylinders
PSD Power spectral density
St Strouhal number
u Reduced flow velocity
U Flow velocity
w Displacement
ζ Damping ratio
μ Dynamic viscosity
ρ Mass density
χ Confinement factor
ω Frequency (rad/s)

INTRODUCTION

Vortex-induced vibration is a term which is almost exclusively referring to cross-flow induced vibrations [1]. However, that does not imply that there cannot be any vortical motion and resulting vibration in purely axial flow conditions. If a dense cluster of cylinders is mounted in axial flow, a flow instability similar to a Kelvin-Helmholtz instability has been observed (e.g. [2–5]). This instability was discovered with the advent of nuclear reactors as the amount of mixing and heat transfer between different subchannels was too high to be explained by turbulent diffusion. At first, it was believed that the enhanced mixing originated from secondary flows driven by the anisotropy of turbulence. Although such secondary flows occur in these bundles, their effect turned out to be small compared to another flow pattern: periodic large-scale vortices [6]. These vortices arise from the interaction of the high-speed flow in the subchannels and the low-speed flow in the gap between cylinders. An overview of the experimental research on large scale vortices in axial flow is given by Meyer [7].

Due to the importance of this phenomenon for the mixing and heat transfer between different subchannels in reactors, also numerical research has been performed. The initial research, based on steady RANS (Reynolds-Averaged Navier-Stokes) simulations, was not very suc-

*Address all correspondence to this author.

TABLE 1: GEOMETRICAL DATA

Parameter	Value
D	0.025m
P	0.0275m
G	0.0025m
L	1.25m
$L_{flexible}$	0.075m

cessful [8]. However, as this phenomenon is a large scale instability, it qualifies of being computed by URANS (unsteady RANS), which was successfully done in following references: [8–12]. In principle, turbulent scale resolving simulations such as Large-Eddy Simulations or Direct Numerical Simulations even offer an increased accuracy, but they require significantly more computing power [11].

This study aims at predicting vibrations occurring in tightly packed rod bundles with axial flow. At first, the flow through such a geometry with 7 cylinders is computed with unsteady Reynolds-Averaged Navier-Stokes simulations. Based on those results, two cases are set up in which one of the cylinders is flexible and the resulting vibration is computed by means of fluid-structure interaction (FSI) simulations. The cases are constructed in such a way that fluid-elastic instabilities are avoided and that all vibration results from the flow instability. It is anticipated that the large-scale vortices give rise to a parametric resonance. Consequently, the FSI-simulations should be able to capture both the flow instability as well as the effect of the mean flow on modal characteristics of the flexible cylinder, which was the topic of earlier studies [13, 14].

METHODOLOGY

The test bundle in this study consists of 7 cylinders as shown in Figure 1. The geometrical parameters are given in Table 1. The inlet and outlet of the domain are periodic and a pressure gradient of 9810 Pa/m is applied. The flow is computed using URANS simulations with the k-omega SST model. The material properties are provided in Table 2. These simulations are performed with rigid cylinders and the results are presented in the following section.

The fluid-structure interaction, which is analyzed in the final section, is computed by coupled CFD-FE (finite element) simulations. In these simulations only one cylinder is flexible (either cylinder 0 or 1) and only a part of its length is flexible.

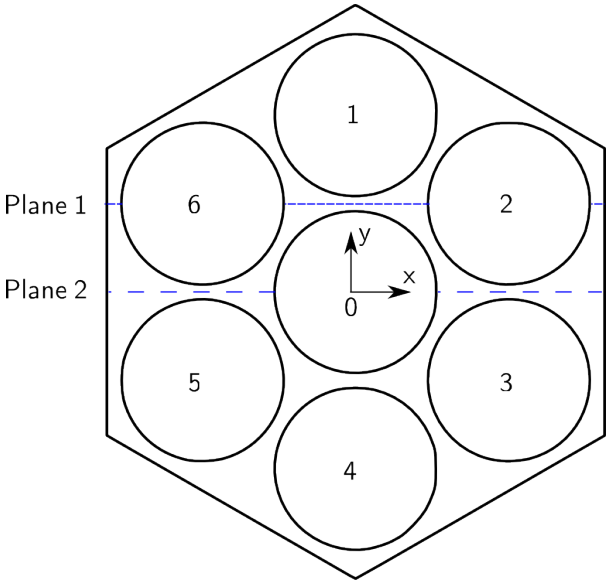

FIGURE 1: SCHEMATIC VIEW OF THE CROSS-SECTION OF THE BUNDLE, WITH INDICATION OF THE POST-PROCESSING PLANE, CYLINDER NUMBERING AND THE COORDINATE SYSTEM.

TABLE 2: MATERIAL PROPERTIES

Property	Value
Fluid density ρ	1000 kg/m^3
Fluid viscosity μ	0.001Pa.s
Youngs elasticity modulus E	750000Pa
Solid density ρ_s	7000kg/m^3

All the equations have been discretized with second order schemes. The fluid grid had 5 radial divisions (from a wall to the middle of the channel), 120 circumferential divisions per cylinder and 480 in streamwise direction. The structural part contains 1350 elements. In order to have a fully developed fluid flow, a settling time of 1.5s has been used. The time step size was 0.289ms.

FLUID DYNAMICS IN ROD BUNDLES

Due to the reduced through-flow area in the gap region between two cylinders, the axial (or z-velocity) is lower in this gap area than in the center of a channel. This is clearly visible in Figure 2, which displays contours of axial velocity in a cross-sectional area. The difference in velocity leads to a flow instability, which is shown in

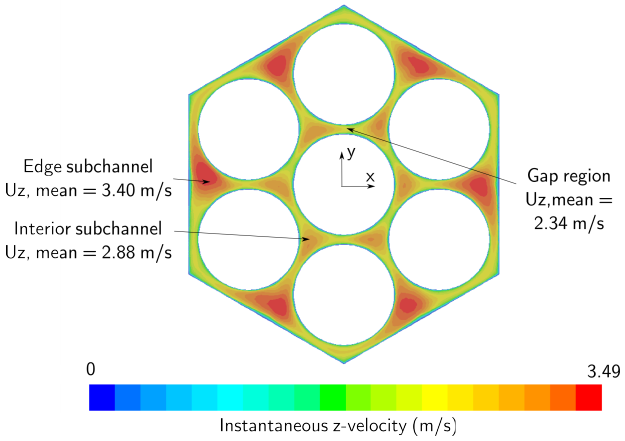

FIGURE 2: CONTOURS OF INSTANTANEOUS Z-VELOCITY (M/S), SHOWING THE DISTRIBUTIONS OF AXIAL VELOCITY IN A CROSS-SECTION.

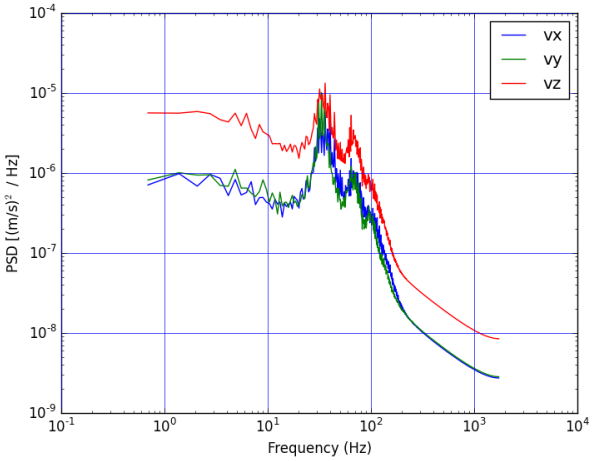

FIGURE 4: POWER SPECTRAL DENSITY OF THE THREE VELOCITY COMPONENTS AVERAGED OVER ALL POINTS IN PLANE 1 AND 2. THE SPECTRUM SHOWS A CLEAR PEAK AROUND 33 HZ, WHICH CORRESPONDS TO THE VORTEX FREQUENCY. A SECONDARY PEAK AT DOUBLE FREQUENCY IS ALSO PRESENT.

Figure 3. This figure shows instantaneous contours of x-, y-, z-velocity and pressure on the two planes defined in Figure 1. The x- and y-axis are oriented as in Figure 1 and the z-axis is oriented along the mean flow direction, which is from left to right. In order for the flow pattern to be visible, only a part of the domain is shown in Figure 2.

As explained in the introduction, a flow instability appears which leads to the wavy character of the axial velocity in Figure 3. Note that the instability occurs in a plane between two cylinders: e.g. plane 2 between cylinder 5 and 6. These periodic large-scale vortices are not only occurring between two adjacent cylinders, but also in the region between a cylinder and the surrounding wall. This explains the oscillations in y-velocity in plane 1 between cylinder 6 or 2 and the wall in Figure 3.

The flow instability is a 2-dimensional instability as can be seen from the x-and y-components of the velocity in Figure 3. The combination of x-z or y-z components shows that the instability contains vortical motions which are transported. The pressure behaves accordingly with low pressure areas in the center of the vortices and high pressure areas outside the center.

Figure 4 displays the power spectral density of the velocity components as a function of frequency. The data are sampled and averaged on both plane 1 and 2. All three components have a clear peak amplitude around 33 Hz. A visual observation of the flow field in the entire domain showed that there were 17 vortices present in the longitudinal direction. Note that the periodicity of the flow boundary conditions imposes an integer number of vortices. Consequently, an uncertainty of at least 0.5/17 is present in these results. The average length of a vortex is thus 1.25 m /17 = 0.0735 m. As these vortices are convected with a velocity close to the bulk velocity in the gap (which is 2.35 m/s), a peak in the Fourier spectrum is expected around 31 Hz, which corresponds reasonably well with the observed peak.

Note that the spectrum also shows a secondary peak at double frequency, corresponding to a smaller flow structure with half the characteristic length of the original one. A second remark is that, according to Möller [4], the sequence of vortices is not necessarily aligned on one axial direction. It is possible that the alternative vortices are created and convected on two axises, slightly off the center axis. However, the hexagonal geometry in this paper is limiting the available space for such a shift.

Influence of Pressure Gradient on Instability

In order to characterize the instability, two parameter sweeps have been performed. In a first parameter sweep, the effect of the mean axial pressure gradient is tested. As the previous paragraph showed that the spectra of the different velocity components contain similar information, only one component (Ux) is analyzed in this paragraph.

It is convenient in this analysis to use non-dimensional parameters. Instead of frequency, the Strouhal number St is used, defined by:

$$St = \frac{fD}{U_c} . \qquad (1)$$

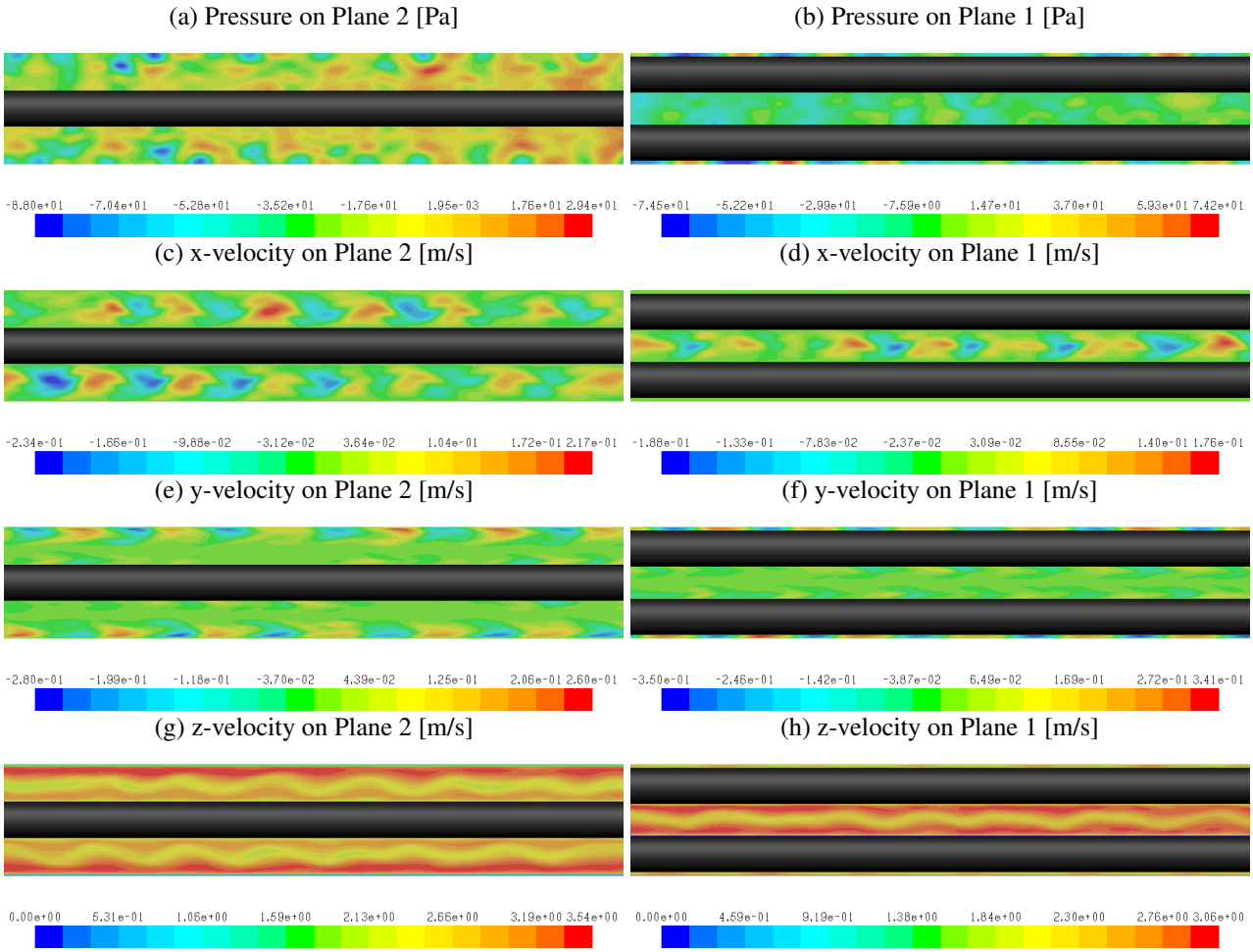

FIGURE 3: VISUALIZATION OF FLOW INSTABILITIES IN ROD BUNDLES. THE FIGURES SHOW (IN DESCENDING ORDER) CONTOURS OF PRESSURE, X-, Y- AND Z-VELOCITY IN PLANE 1 AND 2. THE COORDINATE SYSTEM IS THE SAME AS IN FIGURE 1: THE Z-AXIS POINTS FROM LEFT TO RIGHT AND THE X-AXIS FROM BOTTOM TO TOP.

In this formula U_c is the mean axial velocity. The power spectral density of Ux is also non-dimensionalized by dividing it with the mean axial velocity Uc and the cylinder's diameter.

Figure 5 shows that the pressure gradient has only a very limited influence (within the scatter of the results) on the non-dimensional spectrum. The almost constant Strouhal number implies that the dominant frequency scales approximately linearly with convection velocity. The vertical collapse of the curves in Figure 5 implies that the PSD also scales linearly with convection velocity. This means that the rms-values of Ux (which are the integral of the PSD) also scale linearly with mean convection velocity.

Influence of Pitch-Over-Diameter Ratio on Instability

The second parameter sweep checks the influence of the P/D-ratio on the flow instability. As in the previous paragraph, Figure 6 displays the non-dimensional PSD of Ux versus Strouhal number at different P/D-ratios. In contrast to the previous paragraph, the curves are not coincident.

The rescaled power spectral density decreases with increasing pitch-over-diameter ratio. This behavior can be explained by the following reasoning: with an increasing P/D-ratio, the difference in axial velocity between the gap and subchannel region becomes smaller. As this velocity difference is the driving force behind the flow instability, it becomes weaker with increasing P/D-ratios. At a pitch-over-diameter ratio of 1.3, the instability is at least an order of magnitude weaker than at 1.2 and is almost completely gone. On the other hand, if the gap becomes

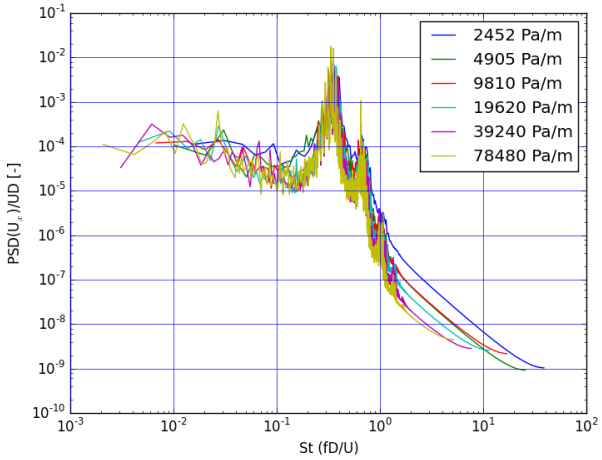

FIGURE 5: EFFECT OF AXIAL PRESSURE GRADIENT ON NON-DIMENSIONALIZED POWER SPECTRAL DENSITY OF UX.

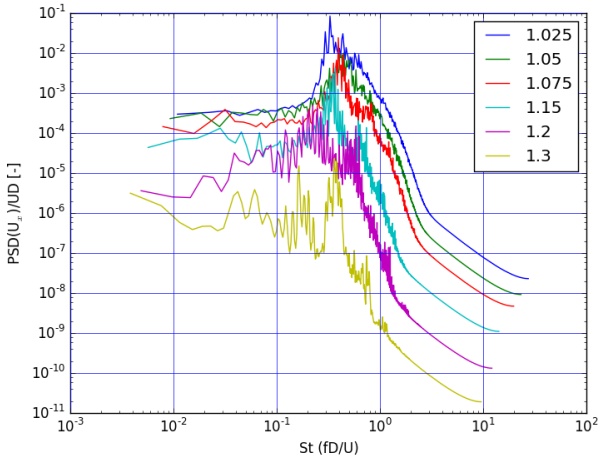

FIGURE 6: NON-DIMENSIONAL POWER SPECTRAL DENSITY OF UX AS FUNCTION OF STROUHAL NUMBER IN BUNDLES WITH VARYING PITCH-OVER-DIAMETER RATIO.

too small, the resistance becomes too large for the fluid to cross the gap and ultimately the large scale vortices will cease to exist. However, this did not happen in the current parameter range.

From correlations in literature [4, 8], it is expected that the peak Strouhal number decreases with increasing P/D-ratio, which is also observed in Figure 6 from P/D = 1.05 to 1.2. However, by comparing both experimental and numerical results in literature, Chang [8] concluded that at very small P/D-ratios the opposite trend occurs. This observation is consistent with the difference in peak Strouhal number at P/D = 1.025 and P/D = 1.05.

FLOW-INDUCED VIBRATION BY LARGE-SCALE PERIODIC VORTICES

Although Figure 3 shows that the flow field on opposite sides of a rod is relatively coherent, large-scale periodic vortices might still trigger vibrations even in beam modes. As described in the methodology section this is tested by performing coupled fluid-structure interaction simulations in which a segment of a cylinder is taken flexible.

Both ends of the flexible segments are clamped to the rigid parts. The length of this piece is chosen to correspond with the wavelength of a typical vortex. The elasticity of the material is chosen in such a way that the reduced flow velocity is sufficiently far from fluid-elastic instabilities. For a clamped-clamped cylinder in axial flow, the limit value is approximately 2π. The reduced flow velocity is defined, with I the second area moment, as

$$u = \sqrt{\frac{\rho \pi D^2 \chi}{4EI}} U_c L \,. \tag{2}$$

Note that this is a slightly modified version of the reduced velocity used in [14]. It takes the effect of flow confinement into account with a confinement factor

$$\chi = \frac{(D+D_H)^2 + D^2}{(D+D_H)^2 - D^2} \,. \tag{3}$$

The mass density of the material is chosen in such a way that the eigenfrequency of the ground mode corresponds to the typical vortex frequency. Two cases are considered: In the first case, a corner cylinder is flexible (cylinder 1 on Figure 1) while in the second case the central cylinder is flexible.

Figure 7 shows the displacement of the center line of the cylinders as a function of time. It demonstrates that the flexible part starts oscillating mainly in a first mode. The amplitude of oscillation is fairly small (up to 1% of the gap width). However, even small amplitude motion can lead to long-term damage. Note that vibrations induced by these vortices might be larger than those induced by turbulence.

A final remark on Figure 7 is that the corner cylinder appears to vibrate more than a central cylinder. This is likely to be a consequence of the asymmetry at the borders. Figure 3 already showed that vortices on both sides

(a) x-displacement central cylinder

(b) y-displacement central cylinder

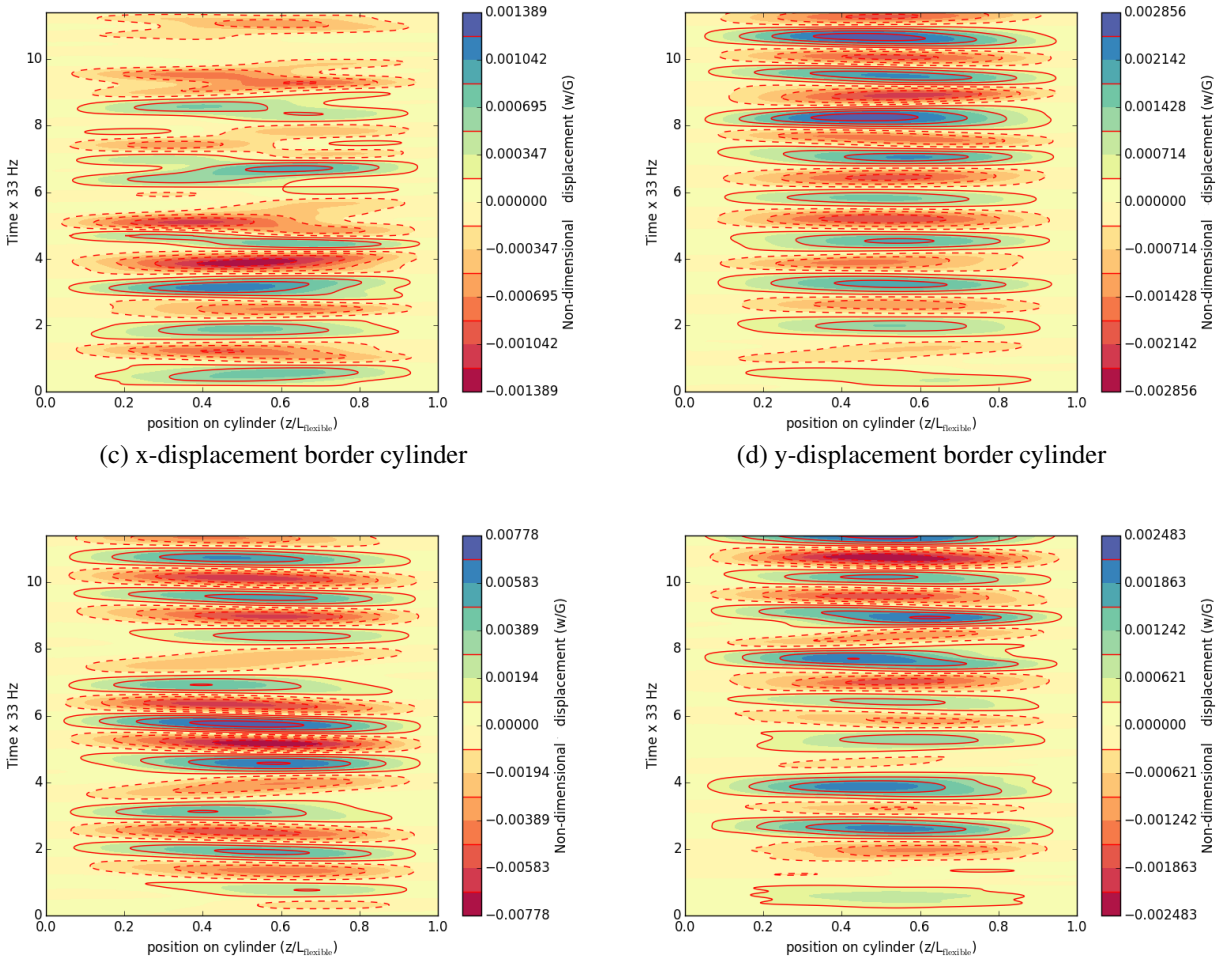

(c) x-displacement border cylinder

(d) y-displacement border cylinder

FIGURE 7: EVOLUTAION OF CENTER LINE DISPLACEMENT NON-DIMENSIONALIZED WITH THE GAP BETWEEN THE CYLINDERS. THE CONTOUR GRAPHS SHOW THAT A FLEXIBLE CYLINDER AT THE BORDER EXPERIENCES MORE VIBRATION THAN A CYLINDER AT THE CENTER.

of the central cylinder are highly correlated, which reduces their strength to trigger beam mode vibrations.

A cylinder at the border of the domain experiences two different type of vortex streets: (type 1) arising from the interaction between the gap and interior subchannels and (type 2) from the interaction between corner subchannel-gap-edge subchannel. The latter vortex street has larger pressure fluctuations than the former one. Cylinder 1 in Figure 1 experiences two type 2 vortex streets. When looking at the same axial coordinate, both streets are typically π rad out of phase. Consequently, the vibration of cylinder 1 in x-direction is stronger than in y-direction.

Influence of Young's Modulus

In this paragraph the influence of Young's modulus on the resulting vibration pattern is tested. Figure 8 shows the maximal displacement of either the central cylinder or a cylinder at the border as a function of the Young's modulus. Every point in this graph is the result of a separate calculation, in which one cylinder is flexible.

The rightmost points in Figure 8 correspond to the vibrations discussed in the previous paragraph. It clearly shows that the outer cylinder vibration has a larger amplitude, which was discussed in the previous paragraph.

Even the leftmost points are still in the fluidelastic stable region, with a reduced velocity = 3.5. It was verified that no divergence occurred in any of the points. This is typically the first instability occurring for a clamped-clamped cylinder. Although the cylinders are in a fluide-

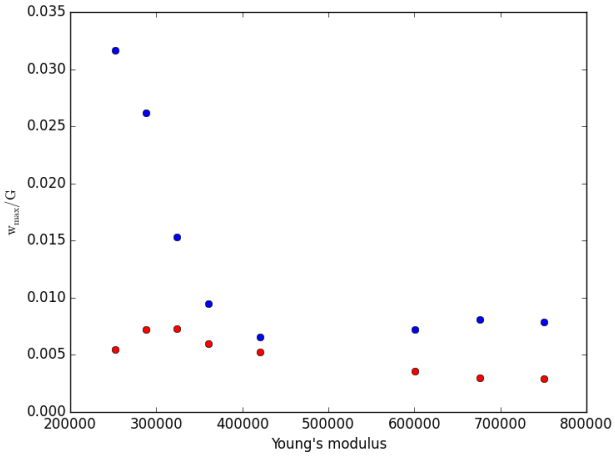

FIGURE 8: MAXIMAL DISPLACEMENT AS A FUNCTION OF YOUNG'S MODULUS. THE BLUE SYMBOLS CORRESPOND TO THE DISPLACEMENT OF CYLINDER 1, WHILE THE RED CIRCLES CORRESPOND TO DISPLACEMENT OF CYLINDER 0. THE RIGHTMOST POINTS CORRESPOND TO A GROUNDMODE VIBRATION OF THE FLEXIBLE CYLINDER, WHILE THE POITNS AT THE LEFT CORRESPOND TO A SECOND MODE VIBRATION.

lastic stable region, Figure 8 shows a second (and higher) maximum at lower Young moduli. In the lowest points, the eigenfrequency of the second beam mode matches the vortex passing frequency. Subsequently, the cylinder is resonating in a second mode.

It is interesting to look at a standard formula for single mode response of a purely sinusoidal excitation, with frequency ω

$$\hat{W}(\omega) = \frac{\hat{F}(\omega)}{M(\omega_n^2 - \omega^2 + 2j\zeta\omega\omega_n)}, \qquad (4)$$

in which $\hat{W}(\omega), \hat{F}(\omega)$ are the Fourier transforms of displacement and force, M is the mass, ω_n the eigenfrequency and ζ the damping ratio. Note that both the first (higher E) and second mode (lower E) resonance occur at the same frequency. Equation 4 then shows that a higher vibrational amplitude can be the result of a lower damping ratio ζ and/or a stronger excitation force, assuming the mass contribution is constant. A decrease in damping ratio is indeed consistent with earlier research [13]. On the other hand, the excitation force is also slightly larger in the second mode vibration, as the vortex pressure profile (with a maximum and minimum per periodic unit) is more similar to a second beam mode vibration.

CONCLUSIONS

This contribution investigated the occurrence of vortex streets caused by axial flow in bundles of cylinders and the vibrations they trigger using numerical simulations. These simulations were able to capture the vortex streets, which originate from the difference in axial flow speed in the gap between cylinders and the subchannel center. It was shown that the Strouhal number and scaled power spectral density remained constant with changing flow velocity. The instability became stronger as the P/D-ratio decreased.

In a subsequent part, fluid-structure interaction simulations predicted the vibration of a flexible cylinder mounted in this bundle. These simulations showed that cylinders at the border of the bundle experienced stronger oscillations. Due to the asymmetry at the border of the hexagonal domain, the vibration occurred in one specific direction. A parameter sweep of the Young's modulus showed that a cylinder with lower stiffness resonated in a second beam mode, with higher amplitude motion. The higher amplitude was caused by a decrease of modal damping ratio and an increase in modal excitation force.

In conclusion, this contribution showed that vortex streets caused by axial flow in an array of cylinders are, under the right conditions, able to trigger beam mode vibrations.

ACKNOWLEDGMENT

This work was performed in the framework of the H2020 SESAME Project. It has received funding from the Euratom research and training program 2014-2018 under grant agreement No 654935 (SESAME). The computational resources (Stevin Supercomputer Infrastructure) and services used in this work were provided by the VSC (Flemish Supercomputer Center), funded by Ghent University, the Hercules Foundation and the Flemish Government department EWI.

REFERENCES

[1] Wu, X., Ge, F., and Hong, Y., 2012. "A review of recent studies on vortex-induced vibrations of long slender cylinders". *Journal of Fluids and Structures,* ***28***(0), pp. 292–308.

[2] Hooper, J. D., and Rehme, K., 1984. "Large-scale structural effects in developed turbulent-flow through closely-spaced rod arrays". *Journal of Fluid Mechanics,* ***145***, pp. 305–337.

[3] Rehme, K., 1992. "The structure of turbulence in rod bundles and the implications on natural mixing

between the subchannels". *International Journal of Heat and Mass Transfer,* ***35***(2), pp. 567–581.

[4] Möller, S. V., 1991. "On phenomena of turbulent-flow through rod bundles". *Experimental Thermal and Fluid Science,* ***4***(1), pp. 25–35.

[5] Meyer, L., and Rehme, K., 1994. "Large-scale turbulence phenomena in compound rectangular channels". *Experimental Thermal and Fluid Science,* ***8***(4), pp. 286–304.

[6] Vonka, V., 1988. "Measurement of secondary flow vortices in a rod bundle". *Nuclear Engineering and Design,* ***106***(2), pp. 191–207.

[7] Meyer, L., 2010. "From discovery to recognition of periodic large scale vortices in rod bundles as source of natural mixing between subchannels-A review". *Nuclear Engineering and Design,* ***240***(6), pp. 1575–1588.

[8] Chang, D., and Tavoularis, S., 2008. "Simulations of turbulence, heat transfer and mixing across narrow gaps between rod-bundle subchannels". *Nuclear Engineering and Design,* ***238***(1), pp. 109–123.

[9] Chang, D., and Tavoularis, S., 2007. "Numerical simulation of turbulent flow in a 37-rod bundle". *Nuclear Engineering and Design,* ***237***(6), pp. 575–590.

[10] Chang, D., and Tavoularis, S., 2012. "Numerical simulations of developing flow and vortex street in a rectangular channel with a cylindrical core". *Nuclear Engineering and Design,* ***243***, pp. 176–199.

[11] Ninokata, H., Merzari, E., and Khakim, A., 2009. "Analysis of low reynolds number turbulent flow phenomena in nuclear fuel pin subassemblies of tight lattice configuration". *Nuclear Engineering and Design,* ***239***(5), pp. 855–866.

[12] Chandra, L., and Roelofs, F., 2011. "CFD analyses of liquid metal flow in sub-channels for Gen IV reactors". *Nuclear Engineering and Design,* ***241***(11), pp. 4391–4403.

[13] De Ridder, J., Degroote, J., Van Tichelen, K., Schuurmans, P., and Vierendeels, J., 2013. "Modal characteristics of a flexible cylinder in turbulent axial flow from numerical simulations". *Journal of Fluids and Structures,* ***43***, pp. 110–123.

[14] De Ridder, J., Doaré, O., Degroote, J., Van Tichelen, K., Schuurmans, P., and Vierendeels, J., 2015. "Simulating the fluid forces and fluid-elastic instabilities of a clamped-clamped cylinder in turbulent axial flow". *Journal of Fluids and Structures,* ***55***, pp. 139–154.